LBNL-50446

SIMULATING UNSATURATED FLOW FIELDS BASED ON GROUND PENETRATING RADAR AND SATURATION MEASUREMENTS

Nils-Otto Kitterød [1] *and Stefan Finsterle*[2]

[1] University of Oslo
Department of Geophysics
Oslo, Norway
nilsotto@geofysikk.uio.no

[2]Lawrence Berkeley National Laboratory
One Cyclotron Road, Mail Stop 90-1116
Berkeley, CA 94720
e-mail: SAFinsterle@lbl.gov

paper presented at the

International Groundwater Symposium
"Bridging the Gap between Measurements and Modeling in Heterogeneous Media" Berkeley, California, March 25–29, 2002

This work was supported—in part—by the U.S. Department of Energy under Contract No. DE-AC03-76SF00098.

Manuscript submitted August 20, 2001 (revised November 29, 2001) to the International Groundwater Symposium "Bridging the Gap between Measurements and Modeling in Heterogeneous Media" Berkeley, California, March 25–29, 2002
Revised April 12, 2002, and submitted to IAHR for publication in special issue of the IAHR Journal dedicated to the International Groundwater Symposium

Simulating Unsaturated Flow Fields Based on Ground Penetrating Radar and Saturation Measurements

Nils-Otto Kitterød[1] and Stefan Finsterle[2]

[1] University of Oslo, Department of Geophysics, ++ 47 228 55825, nilsotto@geofysikk.uio.no
[2] Lawrence Berkeley National Laboratory, Earth Sciences Division, University of California, Berkeley, Califorina

Large amounts of de-icing chemicals are applied at the airport of Oslo, Norway. These chemicals pose a potential hazard to the groundwater because the airport is located on a delta deposit over an unconfined aquifer. Under normal flow conditions, most of the chemicals degrade in the vadose zone, but during periods of intensive infiltration, the residence time of contaminants in the unsaturated zone may be too short for sufficient degradation. To assess the potential for groundwater contamination and to design remedial actions, it is essential to quantify flow velocities in the vadose zone. The main purpose of this study is to evaluate theoretical possibilities and practical limitations of using results from ground penetrating radar (GPR) and measurements of liquid saturation in combination with inverse modeling for the estimation of unsaturated flow velocities. The main stratigraphic units and their geometry were identified from GPR measurements and borehole logs. The liquid saturation measurements reveal the smaller-scale heterogeneities within each stratigraphic unit. The relatively low sensitivity of flow velocities to the observable saturation limits the direct inference of hydraulic parameters. However, even an approximate estimate of flow velocities is valuable as long as the estimate is qualified by an uncertainty measure. A method referred to as simulation by Empirical Orthogonal Functions (EOF) was adapted for uncertainty propagation analyses. The EOF method is conditional in the sense that statistical moments are reproduced independent of second-order stationarity. This implies that unlikely parameter combinations are discarded from the uncertainty propagation analysis. Simple forward simulations performed with the most likely parameter set are qualitatively consistent with the apparent fast flow of contaminants from an accidental spill. A field tracer test

performed close to the airport will be used as an independent dataset to confirm the inverse modeling results.

Introduction

Flow in the vadose zone is decisive for recharge processes and transport of contaminants to the groundwater. Due to spatial heterogeneity in the natural environment and temporal variation in precipitation and evaporation, there are significant practical and theoretical challenges to find a unique set of effective flow parameters that reproduce the main character of the system. A number of field-scale tracer experiments have been conducted in the last decade that elucidate important flow processes in the unsaturated zone (Schulin et al., 1987; Hills et al. 1991; Roth et al. 1991; Flury et al. 1994). A main conclusion is that tracers seem to be transported much more rapidly than expected, and that flow patterns are very irregular. Even in apparently homogeneous soils, flow is observed to be concentrated in very small zones, and a significant portion of released tracers or contaminants are being transported to depth along preferential fast-flow paths. These observations imply that tracer tests in the unsaturated zone are very difficult to monitor and analyze. Nevertheless, tracer tests are considered very valuable, and are used here to confirm the predictive capabilities of a calibrated flow model.

The purpose of this paper is (1) to discuss the possibility of using liquid saturation as the primary data for estimating unsaturated hydraulic parameters, (2) to compare the transport simulations with field tracer test data, and (3) to propose proper orthogonal decomposition for simulation of conditional uncertainties in the estimated flow parameters.

Evaluating liquid saturation as primary data is essential, because this variable can be mapped with high spatial resolution by indirect methods, such as ground penetrating radar tomography (Vasco et al., 1997; Hubbard et al. 1997; Kowalsky et al. (2001), Time Domain Reflectometry (Topp, 1980) or — as done in this project — a combination of neutron scattering measurements and interpolation by kriging (Kitterød et al., 1997). Large-scale flow modeling relies on structural mapping of the geological formation. Because there is a relation between liquid saturation and

hydraulic properties, spatially continuous images of liquid saturation also reflect the geological structure. Parameter estimation is conducted in the framework of the Bayesian Maximum Likelihood method (Carrera and Neuman, 1986). Because orthogonal decomposition is not a very common method in stochastic simulation, we include a brief outline of its mathematical background.

Method

Forward Modeling

The numerical flow simulator TOUGH2 (Pruess, 1991) is used to solve the forward problem. Unsaturated flow is modeled according to Richards' equation (Richards, 1931) with the van Genuchten (1980) constitutive relations describing capillary pressure and relative permeability as a function of saturation.

Inverse Modeling

The inverse problem is solved by using the Bayesian Maximum Likelihood method (Carrera and Neuman, 1986), which is implemented in the inverse modeling code iTOUGH2 (Finsterle, 1999). The parameter set to be estimated is $\mathbf{p} = \{\mathbf{p}_1, \ldots, \mathbf{p}_i, \ldots, \mathbf{p}_N\}$ where N is the total number of geological units (in this case N=4), and $\mathbf{p}_i = \{k_{abs}, S_r, 1/\alpha, n\}_i$, is the vector of hydrogeologic model parameters to be estimated for each unit, k_{abs} [m^2]is absolute permeability; S_r [-] is residual liquid saturation; $1/\alpha$ [Pa] is air entry value; and n [-] is a parameter characterizing the grain size distribution. The parameters are estimated by matching the data, which requires evaluation of the residual at each calibration point:

$$r_j = y_j^* - y_j(\mathbf{p}), \qquad j = 1, \cdots, u \tag{1}$$

Here, y_j^* is the observation at location j in time and space, and y_j is the corresponding value calculated with the forward model for systematic variation of the unknown parameter vector $\mathbf{p}$. If the residual vector $\mathbf{r}=\{r_1,\ldots,r_j, \ldots, r_u\}$ is Gaussian, maximum likelihood estimates are obtained by minimizing an objective function that is the sum of the squared residuals weighted by the inverse of a covariance matrix $\mathbf{C}_{yy}$:

$$Z(\mathbf{p}) = \mathbf{r}^T \mathbf{C}_{yy}^{-1} \mathbf{r} . \quad (2)$$

$\mathbf{C}_{yy}$ represents measurements error and statistical information about the *a priori* information regarding **p**. If $Z(\mathbf{p})$ is properly conditioned, an optimal set of parameters, **p***, exists that minimizes (2), i.e., $Z(\mathbf{p}^*) = \min\{Z(\mathbf{p})\}$. We use the Levenberg-Marquardt algorithm (Press et al., 1992) to find the minimum of the objective function.

For a reasonably small confidence region, y_j is assumed to be a linear function of **p**, in which case the covariance matrix of the estimated parameters is given by (Carrera and Neuman, 1986):

$$\mathbf{C}_{pp} = s_0^2 \left(\mathbf{J}^T \mathbf{C}_{yy}^{-1} \mathbf{J} \right)^{-1} \quad (3)$$

where **J** is the Jacobian sensitivity matrix evaluated at **p***:

$$J_{ij} = -\frac{\partial r_i}{\partial p_j} = \frac{\partial y_i}{\partial p_j} \quad (4a)$$

or scaled with respect to standard deviation of expected parameter variation σ_p and standard deviation of observations σ_y :

$$J' = J_{ij} \frac{\sigma_{p_j}}{\sigma_{y_i}} \quad (4b)$$

The estimated error variance serves as a goodness-of-fit measure:

$$s_0^2 = \frac{Z(\mathbf{p})}{u - v} = \frac{\mathbf{r}^T \mathbf{C}_{yy}^{-1} \mathbf{r}}{u - v} \quad (5)$$

where u is the number of observations, and v is the number of parameters.

Uncertainty Propagation Analysis

Common for all flow problems is the presence of cross-correlations among the parameters, both within each geological unit and between parameters in different

units. A very important result of the inverse modeling procedure is the estimated covariance matrix of the parameters, $\mathbf{C}_{pp}$. In standard forward Monte Carlo simulations, the correlation information in $\mathbf{C}_{pp}$ is usually not taken into account, which means that unlikely parameter combinations are included in the error propagation analysis. The consequence of ignoring the $\mathbf{C}_{pp}$ information give rise to overestimation of the prediction uncertainty.

Based on Gaussian probability theory, we can make use of all the information contained in $\mathbf{C}_{pp}$ and propagate it through a forward model. Decomposing large amounts of correlated observations into eigenfunctions and eigenvalues has been common practice in geosciences since Holmström (1963; 1970). In this tradition the eigenfunctions are called Empirical Orthogonal Functions (EOF), indicating the fact that the covariance matrix has been derived directly from observations. Stochastic simulation by eigenfunctions and eigenvalues is referred to as EOF-simulation (Braud and Obled, 1991; Kitterød and Gottschalk, 1997) or Kahrunen-Loève expansion (Christakos, 1992).

If the estimated parameter set $\mathbf{p}$ is linearly independent, the covariance matrix $\mathbf{C}_{pp}$ can be decomposed into a set of eigenvalues $\boldsymbol{\mu}=\{\mu_1,\ldots,\mu_i,\ldots\mu_v\}$ and eigenvectors $\boldsymbol{\beta}=\{\boldsymbol{\beta}_1,\ldots,\boldsymbol{\beta}_i,\ldots,\boldsymbol{\beta}_v\}$:

$$\mathbf{C}_{pp}\boldsymbol{\beta}^T=\boldsymbol{\mu}\boldsymbol{\beta} \tag{6}$$

According to the proper orthogonal decomposition theorem (Loève, 1977), one stochastic field $x_i(\xi)$ can be generated by expanding the eigenfunctions as follows:

$$x_i(\xi)=\sum_{k=1}^{v}\Phi_k(\xi)\boldsymbol{\beta}_k \qquad i=1,\ldots,v \tag{7}$$

The stochastic coefficients $\Phi_k(\xi)$ are related to the eigenvalues μ_k in a statistically proper sense, which means that $\Phi_k(\xi)$, ($k=1,\ldots,v$) are uncorrelated:

$$\mathrm{E}\{\Phi_i(\xi)\Phi_j(\xi)\} = \delta_{ij}\mu_j \qquad i,j = 1,...,v \tag{8}$$

where $\delta_{ij} = 0$ if $i \neq j$, and $\delta_{ij} = 1$ if $i = j$, and $\Phi_k(\xi)$ is drawn from a Gaussian probability density function, i.e., $\Phi_k(\xi) \in \mathrm{N}(0,\mu_k)$. The eigenvectors are proper in a deterministic sense, which means that they are orthogonal.

In a second step, conditional flow parameters $p_i(\xi)$ are generated:

$$p_i(\xi) = \sigma_i \cdot x_i(\xi) + p_i^* \qquad i = 1,...,v \tag{9}$$

where $\sigma^2_i = \mathrm{Var}[p_i | p_m; m=1,\ldots,i\text{-}1,i\text{+}1\ldots,v]$, i.e., it is a measure of the uncertainty of the estimated parameter i, given the uncertainties of all the other parameters. In this context, σ_i is the square root of the diagonal elements of $\mathbf{C}_{pp}$. In (9), $p_i^* = \mathrm{E}[p_i | p_m; m=1,\ldots,i\text{-}1,i\text{+}1\ldots,v]$ is the conditional expectation of flow parameter i corresponding to the solution $\boldsymbol{p}^*$. Because the covariance matrix $\mathbf{C}_{pp}$ is projected onto the eigenvectors, $\mathbf{C}_{pp}$ is exactly reproduced within a confined confidence interval:

$$\mathrm{E}\left[\left(p_i(\xi) + p_i^*(\xi)\right)\left(p_j(\xi) + p_j^*(\xi)\right), \quad i,j = 1,...,v\right] = {}^{\xi}\mathbf{C}_{pp} = \mathbf{C}_{pp} \tag{10}$$

However, as documented in the case study, some realizations of $\mathbf{p}$ may be outside physical limits, and exact reproduction of $\mathbf{C}_{pp}$ is not possible, thus ${}^{\xi}\mathbf{C}_{pp} \approx \mathbf{C}_{pp}$.

Case study

Geology

The conceptual model is usually developed based on qualitative knowledge of the sedimentological architecture, information that directly affects the inverse modeling results. All field data were sampled at the research site Moreppen at Gardermoen, Norway, close to Oslo Airport. The sediments at the Gardermoen area are part of a marine ice-contact delta system deposited approximately 9500 years ago. The

Moreppen site is located at the distal side of the delta. Based on core samples and excavation of two lysimeter trenches, four sedimentological units were identified, two units in the horizontal topset beds and two units in the foreset beds. The first unit in the topset beds consists of a 10–20 cm thick layer of fine eolian sand that partly penetrates the coarser fluvial sand and gravel. The second topset unit (~2 m thick) consists of delta plain sediments ranging from fine sand (overbank deposits) to coarse riverbed sediments (sorted sand and gravel). The foreset beds are dipping at an angel of approx. 15° with a predominantly northwestern direction, indicating a delta progression in that direction. The dominant foreset unit consists of very well sorted fine to medium sand. The second foreset unit is sandy silt, probably deposited in response to changing channel positions within the river plane. A thorough sedimentological study of the Gardermoen delta is given by Tuttle (1990; 1997).

Data

In this study GPR signals were used to construct the conceptual geological model (fig.1). A pulseEKKO IV system (Sensors and Software, 1993) was used for sampling. The antennas used for mapping structures in the unsaturated zone had a center frequency of 200 MHz and were supplied by a 400 V transmitter. The transmitter and receiving antennas were separated by 1 m. The sampling was done in discrete steps of 0.5 m. Each time series was stacked 64 times in order to increase the signal to noise ratio. Average propagation velocities in the unsaturated zone were 0.12–0.13 m/ns. This was obtained by the conventional Common-Depth-Point method, and is consistent with the reflector from the groundwater table at 70 ns two-way travel time (fig. 1). Approximate vertical resolution is 8–16 cm (i.e., ¼ – ⅛ of a wave length). Assuming that most of the reflected energy comes from the first Freznel zone, the maximum horizontal resolution at 0.5 m and 4.5 m below the surface is 30 cm and 80 cm, respectively. Because the propagation velocities of the electromagnetic wave is a function of the soil moisture content, the GPR signals may be transformed to estimates of liquid saturation by inversion of the propagation velocities. However, to evaluate the reliability of such estimates, liquid saturation should be observed in a more direct way.

In this study liquid saturation was therefore measured by the conventional neutron scattering method (IAEA, 1970). These high-quality data with measurement errors less than 1% volume water (Langsholt, 1993) were used as primary input for inverse modeling to estimate unsaturated flow parameters. The radioactive source generating fast neutrons was americium-beryllium (^{241}Am-Be) with strength 1.11 GBq, and a scintillation detector counted the thermalized neutrons. The source and detector were built into the same equipment, thus only one access tube was necessary to observe the soil moisture content along one vertical line. Twenty-two access tubes were installed within an area of 100 m × 100 m, each with a length of 6 m. To map the spatial variability at a small scale, some of the observation tubes were located close to each other, separated by only 2.5 m (fig. 2). The radii of importance in neutron scattering vary as a function of the soil moisture content. With the water content observed in this study, the radius is estimated to be between 30 and 50 cm.

A time series of effective infiltration was available from the Norwegian Institute of Meteorology. A time series of 17 days was chosen as input to the transient flow simulation. The transient data covered a rainfall event followed by an evapo-transpiration period of 12 days. Steady-state conditions for constant infiltration were simulated preceding the transient rainfall-evapotranspiration event; the applied rate during this initial period is later referred to as the historical steady-state infiltration rate.

Measurements of direct permeability based on core samples, and estimates of hydraulic conductivities from grain size distribution were also available (Pedersen, 1994; Søvik and Aagaard, 2001). Laboratory measurements of pressure and saturation were performed on small (~75 cm^3) core samples and plotted as characteristic curves (Pedersen, 1994). All these independent observations were included as *a priori* information weighted by the respective experimental variance.

Inverse Modeling Results

Firstly, uncertainties in the conceptual geological model were investigated by varying the interfaces between the units. The sedimentological architecture was refined based on insight into the system behavior as a result of the imposed changes, until the

differences between observed and calculated liquid saturations were minimized. For each realization of the sedimentological architecture, a new set of optimal parameters was estimated. Figure 3 illustrates the stepwise refinement of the sedimentological architecture. The corresponding deviation between observed and calculated saturations is given in fig. 4.

Another question of practical interest is the importance of having spatially continuous observations (e.g., from tomographic analyses) versus limited observations from vertical boreholes. Preliminary inversions comparing continuous observations with borehole observations at a given point in time were performed. Different infiltration scenarios were evaluated, with steady-state and transient infiltration at different rates. A significant improvement in estimation results is achieved when transient infiltration fluxes were entered, whereas the historical steady-state infiltration intensity had no significant impact on the inversion results (fig. 4).

The scaled sensitivities J'_{ij} in fig. 5 show that if there are observations of liquid saturation in the units where parameters are estimated, all scaled sensitivities are above one except for unit top 1 where only two observations were included (one observation point per well). The scaled sensitivity with respect to absolute permeability in top 1 and the air entry value of top 1 was very low. The latter parameter was omitted in the final inverse modeling procedure. The sensitivity analysis indicates that the particular problem is sufficiently well conditioned if there are more than two (or a few) liquid saturation measurements in the units where parameter estimates are required. It should be emphasized, however, that consistency between geological architecture and liquid saturations are carefully controlled, and that we had *a priori* information on parameter values. For some parameters liquid saturations were sensitive also across sedimentological units. The air entry value ($1/\alpha$ in fig. 5) and the grain size distribution parameter (vG_n in fig. 5) in top 2 is of importance in dip 1, while the air entry value of dip 1 has impact on the saturations in top 2. For obvious reasons the parameters in dip 2 have no influence on the saturations in top 1 or top 2. Dip 2 is very thin compared to top 2 and dip 1. With respect to saturations the most important observations are those in the dip 1 unit.

Tracer Test

Three well-monitored field-scale tracer tests have been performed at the Moreppen site. The tests focused on microbiological degradation of de-icing chemicals (Swensen, 1997; French, 1999) and transport and degradation of hydrocarbons (Søvik et al., 2001). In the latter experiment two conservative tracers were applied, tritiated water (HTO) and bromide (Br^-). The tracer test covered an area of 3 m × 6 m. Infiltration of 30 mm/day was applied for 7 days to approximately achieve steady-state conditions prior to the release of tracers. Br^- was then added through a 3 m long line at a rate of 300 l/day for 3 days. At the same time, background infiltration was increased to 43 mm/day. Tritiated water was applied later during the experiment. Figure 6 shows the measured breakthrough curves for HTO and Br^-. The difference in travel times between HTO and Br^- are probably due to slightly different field saturations.

Breakthrough curves were first simulated based on the best-estimate parameter set determined by inverse modeling as described above. In the preliminary simulations absolute permeability was simulated as an isotropic parameter. However, it is not very likely that permeability is isotropic. A preliminary simulation shows clearly that observed velocities in the topset are higher than the model predictions. The opposite is true for velocities in the foreset unit. For this reason anisotropy was included as a constant factor in the final inversions. Due to the very coarse grained material in the topset unit, partly degraded roots and other hydraulic impact from vegetation, we expect a higher vertical permeability in the topsets. In the foresets there is significant layering that reduce the vertical permeability. The horizontal to vertical permeability ratio was therefore set equal to 1:10 in the topset, and 100:1 in the foresets. Those anisotropy factors cannot be considered as true *a priori* information, but we feel there are good physical reasons to include anisotropy. The simulated breakthrough curves (fig. 6) indicate that even though the vertical permeability is ten times higher than the horizontal permeability, the travel times in the topset unit is still overestimated.

Error Propagation Analysis

Simulations based on the EOF method are presented here for layer ‘dip 2’ only (see fig. 3). 500 stochastic fields of the four parameters k_{abs}, S_r, $1/\alpha$, and n were drawn

from a distribution that is consistent with the covariance matrix $\mathbf{C}_{pp}$. The resulting saturations as calculated by the forward models are summarized in a histogram. In a second analysis based on the same procedure, the correlations of the $\mathbf{C}_{pp}$ matrix were neglected. As clearly demonstrated in fig.7, the simulated uncertainties are significantly reduced by the EOF-simulation. Reproduction of $\mathbf{C}_{pp}$ is almost perfect if the simulated parameters are allowed to span an unlimited outcome domain (fig.8). However, because some of the parameters may fall outside the physically feasible parameter space, the outcome domain has to be truncated, and $\mathbf{C}_{pp}$ is not accurately reproduced. Note that in these cases, the applicability of the linearity assumption must be questioned.

Conclusion

The main purpose of this study was to evaluate the possibility of using liquid saturation as primary input data to inverse modeling to determine unsaturated flow parameters. Numerous previous studies have demonstrated that saturation is not very sensitive to the flow parameters of interest. Kool and Parker (1988) pointed out that pressure data are twice as sensitive as saturation data. We wanted to examine whether an increase of the spatial density of observations could overcome some of the insufficiency associated with saturation data. We evaluated the problem by comparing the inverse modeling results using either continuous observations of liquid saturation or discrete observations from boreholes only. This question is of great interest as it assesses the potential usefulness of high-resolution radar data. Spatially continuous observations of soil moisture content may be available at low costs in the near future, either from borehole tomography with very high spatial resolution, or from ground penetrating radar surveys. Satellites equipped with low frequency radar technology may also be a potential source for large-scale observations of soil moisture content in the future.

The present study indicates that observations of liquid saturation alone are not sufficient. Independent information about the geological framework is necessary, along with independent information of the flow parameters. A small perturbation in the *a priori* information results in different estimation results, indicating that the

inversions of saturation data are strongly conditioned on prior information. Furthermore, inaccuracies in specifying unit interfaces may have introduced systematic errors, highlighting the importance of the sedimentological framework model. The simulated tracer test indicates, however, that the derived flow parameters are reasonable. Recall that the observations from the tracer test are not included in the inverse modeling procedure, i.e., they serve as an independent test of the appropriateness of the calibrated flow model.

Finally, the preliminary evaluation of the EOF simulation reveals the importance of including the $\mathbf{C}_{pp}$ matrix in the error propagation analysis. The EOF method discards unlikely parameter combinations, thus reducing prediction uncertainties. Note that EOF as presented here applies to Gaussian stochastic processes. Unlike many other methods, the assumption of second order stationarity of statistical moments is not necessary. Because the eigenfunctions ensure approximate reproduction of the $\mathbf{C}_{pp}$ matrix directly, the simulation algorithm is also very fast.

Acknowledgments

We greatly acknowledge Anne Kristine Søvik and Eli Alfnes and their co-authors for giving us access to their data and explain to us every detail of the field tracer experiment. This study was a part of "The Gardermoen project", funded by the Reseach Council of Norway and the Norwegian Civil Aviation Authorities. This work was supported—in part—by the U.S. Department of Energy under Contract No. DE-AC03-76SF00098.

References

Braud, I., and C. Obled, 1991. On the use of Empirical Orthogonal Function (EOF) analysis in the simulation of random fields. Stochastic Hydrol. Hydraul. 5, 125—124.

Carrera, J. and S. P. Neuman, 1986. Estimation of Aquifer Parameters Under Transient and Steady State Conditions: 1. Maximum Likelihood Method incorporating prior information Water Resour. Res., (22) 2, 199—210.

Christakos, G., 1992. Random Field Models in Earth Sciences, 474 pp., Academic Press, Inc.U.S.A ISBN 0-12-174230-X.

Finsterle, S., 1999. iTOUGH2 user's guide, ,Report LBNL-40040, Lawrence Berkeley National Lab., Berkeley, California.

Flury, M, H., Flühler, W.A. Jury, and J. Leuenberger, 1994. Susceptibility of soils to preferential flow of water: A field study, Water Resour. Res., 30(7), 1954—1954.

French H., 1999. Transport and degradation of deicing chemical in a heterogeneous unsaturated soil, Ph.D. thesis, Agricultural University of Norway, ISBN 82-575-0394-0.

Genuchten, van M.T., 1980. A closed-form equation for predicting the hydraulic conductivity of unsaturated soils, Soil Sci. Am. J., 44, 892–898.

Hills, R.G., P.J. Wierenga, D.B. Hudson, and M.R. Kirkland, 1991. The second Las Cruces trench experiment: Experimental results and two dimensional flow predictions, Water Resour. Res., 27(10), 2707—2718.

Holmström, I. (1963). On the method for parametric representation of the state of the atmosphere, Tellus, XV, 127-149.

Holmström, I. (1970). Analysis of time series by means of empirical orthogonal functions, Tellus, XXII, 638-647

Hubbard, S.S., Y. Rubin, and E. Majer, 1997. Ground-penetrating radar-assisted saturation and permeability estimation in bimodal systems, Water Resour. Res., 33(5), 971—990.

IAEA (International Atomic Energy Agency) 1970. Neutron Moisture Gauges, 96 pp., Technical report series No. 112, STI/DOC/10/112, Vienna, Austria.

Kitterød, N.-O, E. Langsholt, W.K. Wong, and L. Gottschalk, 1997. Stochastic interpolation of soil moisture, Nordic Hydrology, 28(4/5), 307—328.

Kitterød, N.-O. and L. Gottschalk, 1997. Simulation of normal distributed smooth fields by Karhunen- Loève expansion in combination with kriging, Stoch. Hydrol. and Hydaul. 11, 459–482.

Kool, J.B., and J. C. Parker, 1988. Analysis of the Inverse Problem for Transient Unsaturated Flow, Water Resour. Res., 24 (6) 817—830.

Kowalsky, M.B., P. Dietrich, G. Teutsh, and Y. Rubin, 2001. Forward modeling of ground-penetrating radar data using digitised outcrop images and multiple scenarios of water saturations, Water Resour. Res., 37 (6) 1615—1625

Langsholt, E., 1993. Kalibrering av nøytronmeter Moreppen, oktober 1993 (Calibration of neutronmeter Moreppen october 1993, in Norwegian) Reportseries B(4), University of Oslo, Oslo, Norway.

Loève, M., 1977. Probability Theory II, ISBN: 0-387-90210-4, Springer-Verlag, New York, New York.

Pedersen, T.S., 1994. Væsketransport i umettet sone. (Water transport in the unsaturated zone). In Norwegian, Cand. Scient thesis, Dept. of Geology, University of Oslo. The environment of the subsurface-The Gardermoen project, Reportseries C, nr.2, 122 pp.

Pruess, K., 1991. TOUGH2—A general-purpose numerical simulator for multiphase fluid and heat flow, Report LBL-29400, Lawrence Berkeley Laboratory, Berkeley, California.

Press W. H., S.A. Teukolsky, W.T. Vetterling, and B. P. Flannery, 1992. Numerical recipes in C, 2nd ed, ISBN 0 521 43108 5, Cambridge University Press.

Richards, L. A., 1931. Capillary condition of liquids through porous mediums, Physics, 1:318–333.

Roth, K., W.A. Jury, H. Flühler, and W. Attinger, 1991.Transport of chloride through an unsaturated field soil, Water Resour. Res., 27(10), 2533—2541.

Swensen, B., 1997. Transport processes and transformation of urea-N in the unsaturated zone of a heterogeneous, mineral sub-soil, Ph.D. thesis, Agricultural University of Norway, ISBN: 82-575-0300-2.

Schulin, R., van M.Th. Genuchten, H. Flühler, and P. Ferlin, 1987. An experimental study of solute transport in a stony field soil, Water Resour. Res., 23(9), 1785—1794.

Sensors and Software, 1993. PulseEKKO IV user's guide.

Søvik A. K., E. Alfnes, T. S. Pedersen and P. Aagaard, 2001. Funneled transport and degradation of jet fuel contaminated water in the unsaturated zone at a heterogeneous field site. 1. Experimental set up and water flow (submitted to Jour. of Environmental Quality).

Søvik, A.K., and P. Aagaard, 2001. Spatial variability of a solid porous framework with regard to chemical and physical properties, Submitted to European Journal of Soil Science.

Topp, C.G., J.L. Davis, and A.P. Annan, 1980. Electromagnetic determination of soil water content, measurements in coaxial transmission lines. Water Resour. Res., 16, 574—582.

Tuttle, K. J., 1990. A sedimentological, stratigraphical and geomorpholgical inverstigation of the Hauerseter delta and a hydrologigal study of the westerly Øvre Romerike aquifer, Cand. Scient thesis in Geology, Department of Geology, University of Oslo, Oslo, Norway.

Tuttle, K. J., 1997. Sedimentological and hydrogeological characterisation of a raised ice-contact delta – the Preboreal delta-complex at Gardermoen, southeastern Norway, Ph.D. thesis, Department of Geology, University of Oslo, Oslo, Norway.

Vasco D. W., J.E. Peterson, and K. H. Lee, 1997. Ground-penetrating radar velocity tomography in heterogeneous and anisotropic media, Geophysics, (62) 6, 1758—1773.

Wessel, P. and W. H. F. Smith, 1999. The generic mapping tool GMT, version 3.3.3, Technical reference and cookbook, School of Ocean and Earth Science and Technology, University of Hawai'i at Mānoa.

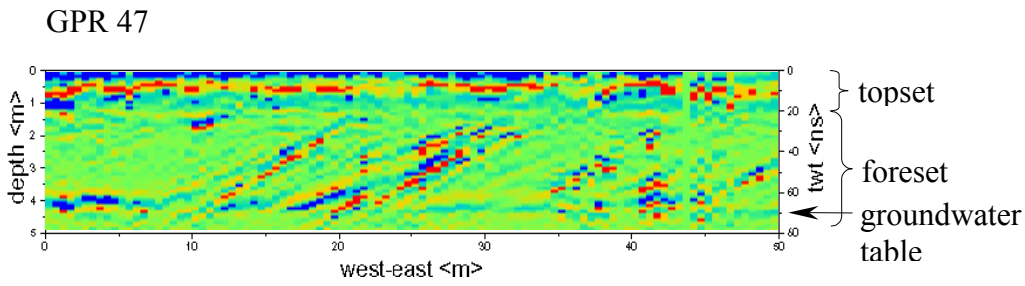

Figure 1. Ground penetrating radar (GPR) signals, profile 47 cf. fig.2. The strong reflectors in the dipping foreset unit is from silty layers with high soil moisture content. Yellow and green reflect drier sand.

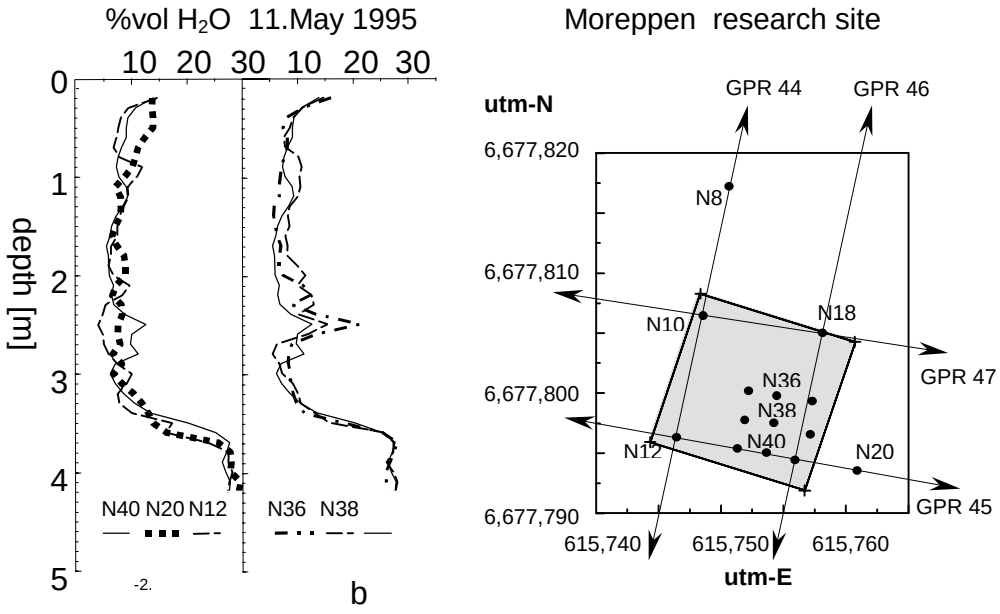

Figure 2. Soil moisture observations plotted along dip direction in a) and along strike direction in b). GPR 47 is given in fig. 1. The pike in soil moisture content at 2.5 m correspond to a strong reflection in the foreset unit.

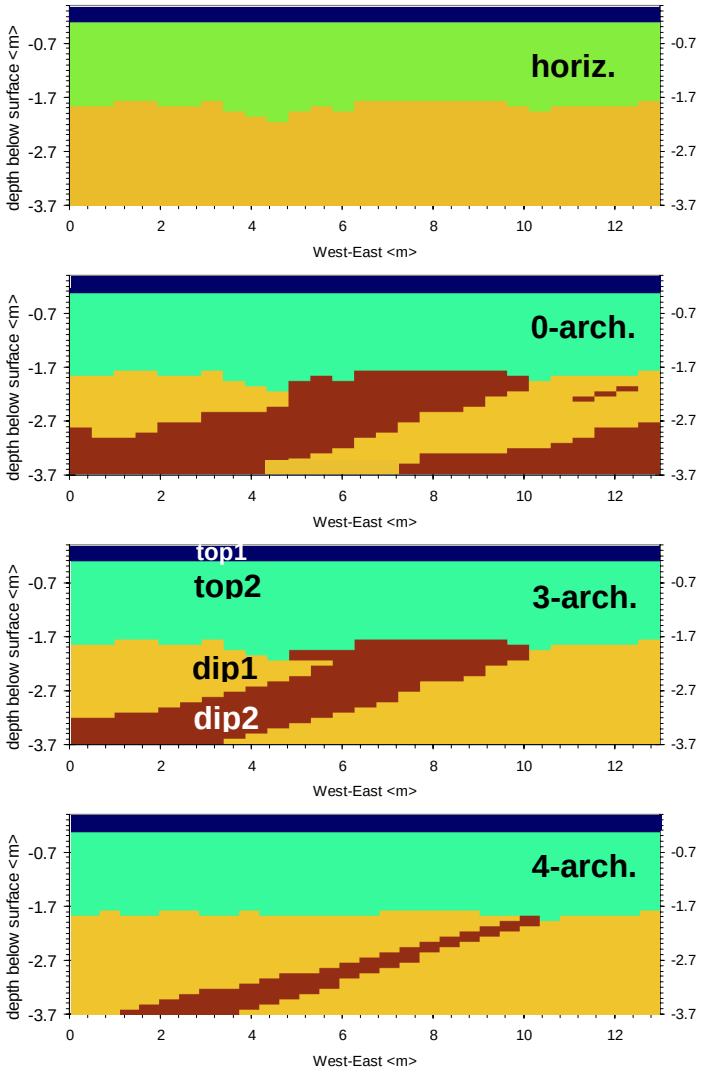

Figure 3. Different sedimentological architectures. Horizontal layering; initial guess (0-arch.); after three refinements (3-arch.); and final refinement (4-arch.).

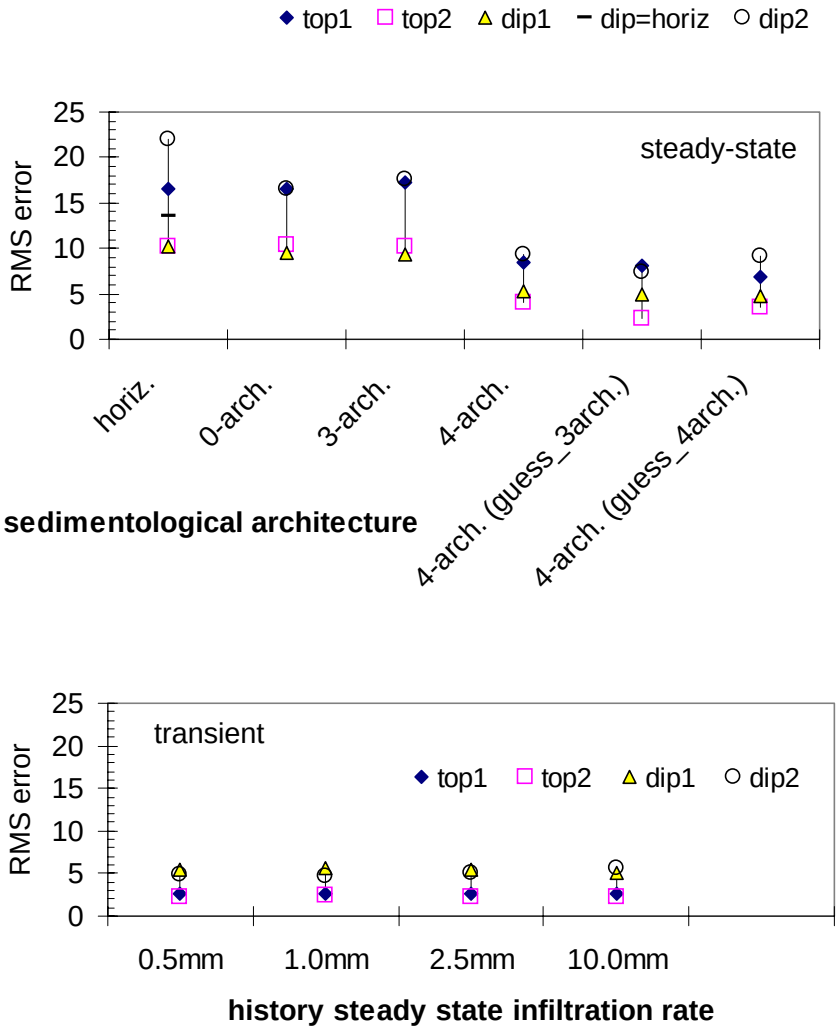

Figure 4. Deviation (Root Mean Square error) between observed and calculated liquid saturations for different sedimentological achitectures at steady state (upper) and for transient infiltration but with different historical steady state infiltration (lower). For steady-state (4-arch.), different intial guesses of parameters had minor impact on the RMS error. Changes in historical steady-state infiltration had also a minor impact on the error. Note the significant improvement when performing transient modeling compared to steady-state simulations.

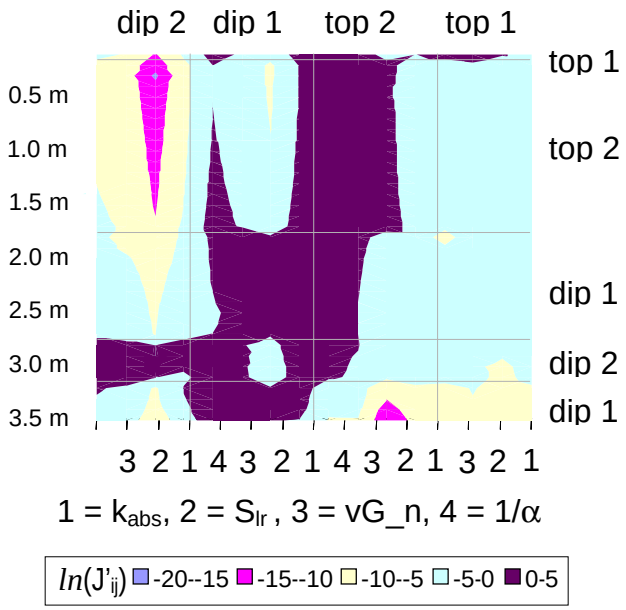

Figure 5. Logarithm of scaled sensitivities (eq. 4b). Parameters are divided into stratigraphical units top 1, top 2, dip 1 and dip 2 along horizontal axis. Vertical axis corresponds to observation point (depth below surface), and is also subdivided according to stratigraphical unit.

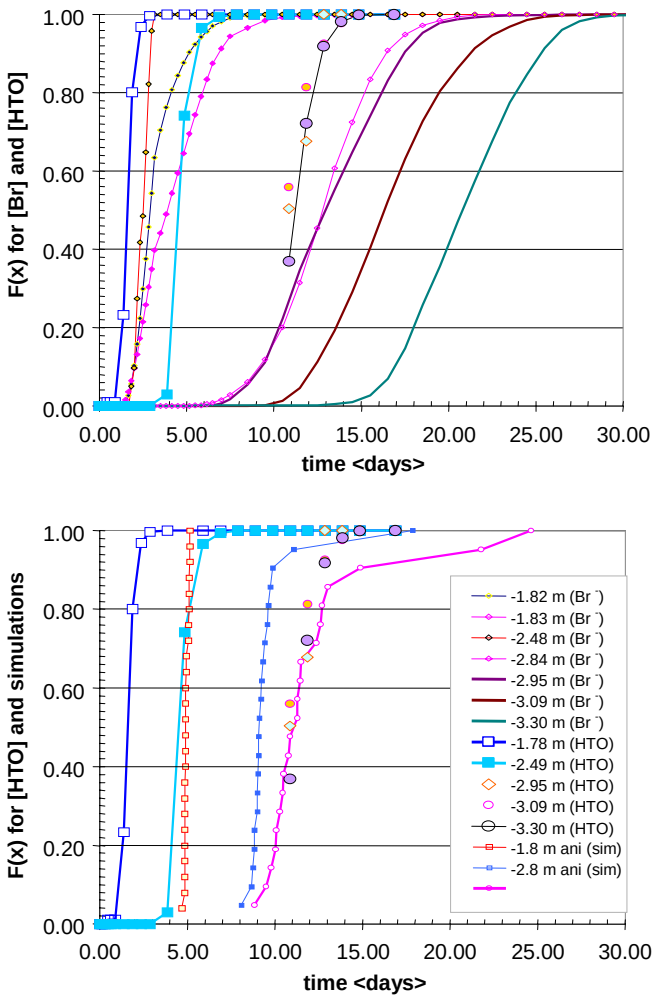

Figure 6. At the top is observed breakthrough curves for bromide (Br^-) and tritiated water (HTO) for the Søvik and Alfnes et al. (2001) tracer test. All observation points are normalized with respect to mass balance. The simulated breakthrough curves are plotted below together with the HTO data. Only advection is taken into account in the simulations. The legend indicates depths [m] of observation or simulation point below surface.

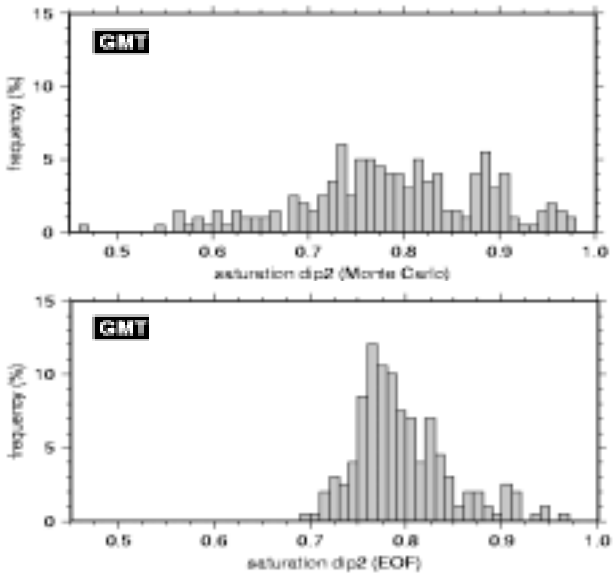

Figure 7. Historgrams of simulated saturations. The upper histogram is produced by simple Monte Carlo simulation where only expected value and variance are included. The lower histogram summarizes EOF simulation results in which the correlations among the parameters are taken into account. Because unlikely parameter combinations are discarded, the uncertainty is narrowed. The historgrams are produced by the Generic Mapping Tools (GMT, Wessel and Smith, 1999).

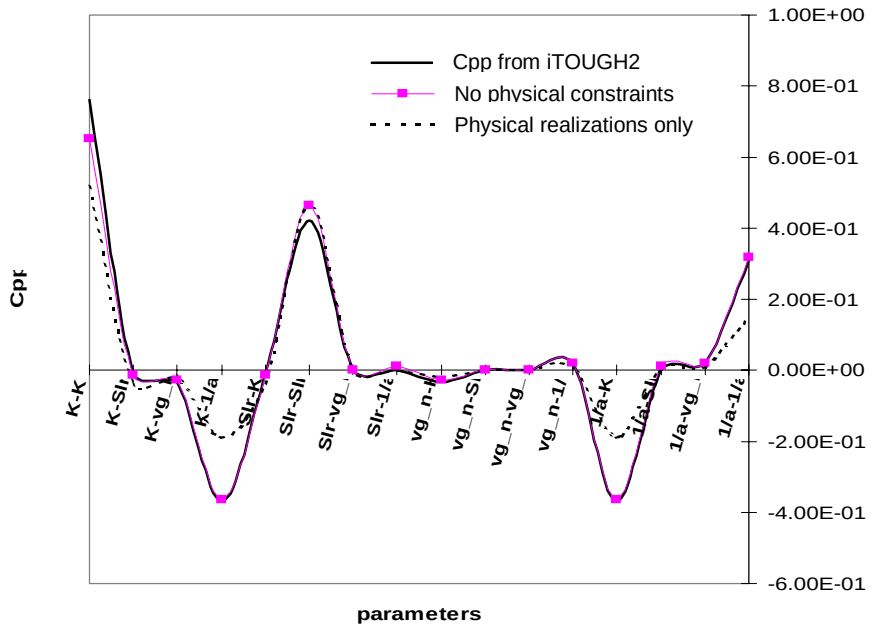

Figure 8. Comparison between the desired input $\mathbf{C}_{pp}$ matrix and the covariance matrix generated by EOF. If no physical constraints are imposed, the simulated parameter values accurately reproduce the given $\mathbf{C}_{pp}$ matrix. Some of the simulated $1/\alpha$ values were outside physical limits. Observing the physical constraints leads to more realistic parameter sets, but a somewhat poorer reproduction of the given covariance matrix.